C E RABINSON

AEDC-TR-76-70

EVALUATION OF REYNOLDS NUMBER AND TUNNEL WALL POROSITY EFFECTS ON NOZZLE AFTERBODY DRAG AT TRANSONIC MACH NUMBERS

PROPULSION WIND TUNNEL FACILITY
ARNOLD ENGINEERING DEVELOPMENT CENTER
AIR FORCE SYSTEMS COMMAND
ARNOLD AIR FORCE STATION, TENNESSEE 37389

July 1976

Final Report for Period January 29, 1974 – October 10, 1974

Prepared for

DIRECTORATE OF TECHNOLOGY (DY)
ARNOLD ENGINEERING DEVELOPMENT CENTER
ARNOLD AIR FORCE STATION, TENNESSEE 37389

NOTICES

When U. S. Government drawings specifications, or other data are used for any purpose other than a definitely related Government procurement operation, the Government thereby incurs no responsibility nor any obligation whatsoever, and the fact that the Government may have formulated, furnished, or in any way supplied the said drawings, specifications, or other data, is not to be regarded by implication or otherwise, or in any manner licensing the holder or any other person or corporation, or conveying any rights or permission to manufacture, use, or sell any patented invention that may in any way be related thereto.

Qualified users may obtain copies of this report from the Defense Documentation Center.

References to named commercial products in this report are not to be considered in any sense as an endorsement of the product by the United States Air Force or the Government.

This report has been reviewed by the Information Office (OI) and is releasable to the National Technical Information Service (NTIS). At NTIS, it will be available to the general public, including foreign nations.

APPROVAL STATEMENT

This technical report has been reviewed and is approved for publication.

FOR THE COMMANDER

Elton R. Thompson

ELTON R. THOMPSON
Research & Development
Division
Directorate of Technology

Robert O Dietz

ROBERT O. DIETZ
Director of Technology

REPORT DOCUMENTATION PAGE		READ INSTRUCTIONS BEFORE COMPLETING FORM
1. REPORT NUMBER AEDC-TR-76-70	2. GOVT ACCESSION NO.	3. RECIPIENT'S CATALOG NUMBER
4. TITLE *(and Subtitle)* EVALUATION OF REYNOLDS NUMBER AND TUNNEL WALL POROSITY EFFECTS ON NOZZLE AFTERBODY DRAG AT TRANSONIC MACH NUMBERS		5. TYPE OF REPORT & PERIOD COVERED Final Report-January 29, 1974 - October 10, 1974 6. PERFORMING ORG. REPORT NUMBER
7. AUTHOR(s) C. E. Robinson, ARO, Inc.		8. CONTRACT OR GRANT NUMBER(s)
9. PERFORMING ORGANIZATION NAME AND ADDRESS Arnold Engineering Development Center (DY) Air Force Systems Command Arnold Air Force Station, Tennessee 37389		10. PROGRAM ELEMENT, PROJECT, TASK AREA & WORK UNIT NUMBERS Program Element 65807F
11. CONTROLLING OFFICE NAME AND ADDRESS Arnold Engineering Development Center (DYFS) Arnold Air Force Station, Tennessee 37389		12. REPORT DATE July 1976 13. NUMBER OF PAGES 36
14. MONITORING AGENCY NAME & ADDRESS(if different from Controlling Office)		15. SECURITY CLASS. (of this report) UNCLASSIFIED 15a. DECLASSIFICATION/DOWNGRADING SCHEDULE N/A

16. DISTRIBUTION STATEMENT *(of this Report)*

Approved for public release; distribution unlimited.

17. DISTRIBUTION STATEMENT *(of the abstract entered in Block 20, if different from Report)*

18. SUPPLEMENTARY NOTES

Available in DDC

19. KEY WORDS *(Continue on reverse side if necessary and identify by block number)*

tests	porosity	Mach numbers
Reynolds numbers	nozzle afterbody (NAB)	
tunnel	drag	
walls	transonic flow	

20. ABSTRACT *(Continue on reverse side if necessary and identify by block number)*

An experimental investigation was conducted to study the effects of Reynolds number variation on isolated nozzle afterbody performance. A strut-mounted cone-cylinder model with three separate afterbody configurations (specified by the Advisory Group for Aerospace Research and Development (AGARD)) was used for this investigation. This program was conducted in two phases distinguished by the model size and the wind tunnels used to

DD FORM 1 JAN 73 1473 EDITION OF 1 NOV 65 IS OBSOLETE

20. ABSTRACT (Continued)

obtain the experimental results. Phase I was conducted in the AEDC Propulsion Wind Tunnel (16T) (Tunnel 16T) over a model length Reynolds number range from 10 x 10^6 to 60 x 10^6 at Mach numbers from 0.6 to 1.5. Phase II was conducted with a model which was a 0.15-percent scale of the Phase I model. The tests were conducted in the Lockheed-Georgia Compressible Flow Facility (CFF) and the AEDC Tunnel 16T. The ranges of Reynolds number and Mach number investigated were 10 x 10^6 to 90 x 10^6 and 0.6 to 1.1, respectively. The effect of tunnel wall porosity on nozzle afterbody (NAB) performance was also investigated during Phase II. Experimental results were obtained at wall porosities of 2, 4, and 6 percent over the previously stated Reynolds number and Mach number ranges in the CFF. The results from both Phase I and Phase II were similar. The drag of the nozzle afterbody increases slightly with increasing Reynolds number. The rate of increase in drag with Reynolds number increases as Mach number increases. The effect of tunnel wall porosity also increased with increasing Mach number and is of the same order of magnitude as the Reynolds number effect.

AFSC
Arnold AFS Tenn

PREFACE

The work reported herein was conducted by the Arnold Engineering Development Center (AEDC), Air Force Systems Command (AFSC), under a cooperative program sponsored jointly by AEDC and the Air Force Flight Dynamics Laboratory (AFFDL), AFSC, under Program Element 65807F. The Air Force project engineer was E. R. Thompson, AEDC/DYR. The results presented were obtained by ARO, Inc. (a subsidiary of Sverdrup & Parcel and Associates, Inc.), contract operator of AEDC, AFSC, Arnold Air Force Station, Tennessee. The work was conducted under ARO Project numbers PA411-21TA and P32P-11A, and the data analysis was completed on October 15, 1975. The author of this report was C. E. Robinson, ARO, Inc. The manuscript (ARO Control No. ARO-PWT-TR-75-157) was submitted for publication on November 3, 1975.

CONTENTS

ILLUSTRATIONS

Figure

Figure Page

TABLES

1.0 INTRODUCTION

An extensive effort to determine the effect of Reynolds number on nozzle afterbody (NAB) performance is currently being conducted, both analytically and experimentally, throughout the aerospace industry. This effort has been made necessary by the increasing aircraft size and operating envelope which make it more difficult to test model configurations in the existing wind tunnels at Reynolds numbers approaching full scale.

In order to gain an insight into the fundamental mechanisms of the effects of Reynolds number on the performance of nozzle afterbodies, the effects can best be investigated on isolated NAB configurations that are free of the influences of the aircraft wings, tail assemblies, and wide-body fuselages. An axisymmetric cone/cylinder model with interchangeable afterbody geometries is frequently chosen to investigate the isolated NAB performance. For most analytical efforts, an axisymmetric model is also chosen because of its simplicity.

An extensive experimental investigation was formulated and has been initiated by AEDC utilizing the axisymmetric cone/cylinder model with afterbody geometries specified by the AGARD Working Group. The program was a many-faceted effort designed to investigate the effect of afterbody shape, exhaust plume temperature (Ref. 1), exhaust plume initial inclination angle (Ref. 2), and Reynolds number and tunnel wall porosity on afterbody pressure drag in transonic flow. The results of the Reynolds number and tunnel wall porosity investigations are presented in this report.

2.0 APPARATUS

The AEDC Reynolds number and tunnel wall porosity investigations were conducted in two phases using two models, one being nominally a 0.15-scale model of the other. The investigation was conducted in two wind tunnels: the Propulsion Wind Tunnel (16T)-(Tunnel 16T) at the Arnold Engineering Development Center (AEDC) and the Lockheed Compressible Flow Facility (CFF) at Lockheed-Georgia.

2.1 WIND TUNNELS

2.1.1 AEDC-Tunnel 16T

Tunnel 16T is a continuous flow, closed-circuit, transonic wind tunnel with a fixed wall porosity of 6 percent, which is capable of being operated within a Mach number range from 0.20 to 1.6. Tunnel 16T can be operated within a Reynolds number range from 0.5×10^6 to 5.5×10^6/ft with a stagnation temperature variation capability from approximately 80°F to a maximum of 160°F. The test section of Tunnel 16T is 16 ft square with a test section length of 40 ft. Figure 1 is a photograph of the experimental

article installed in Tunnel 16T. Tunnel air is removed and replaced with conditioned makeup air from an atmospheric drier to control the specific humidity of the tunnel air. Reference 3 presents a complete calibration of Tunnel 16T.

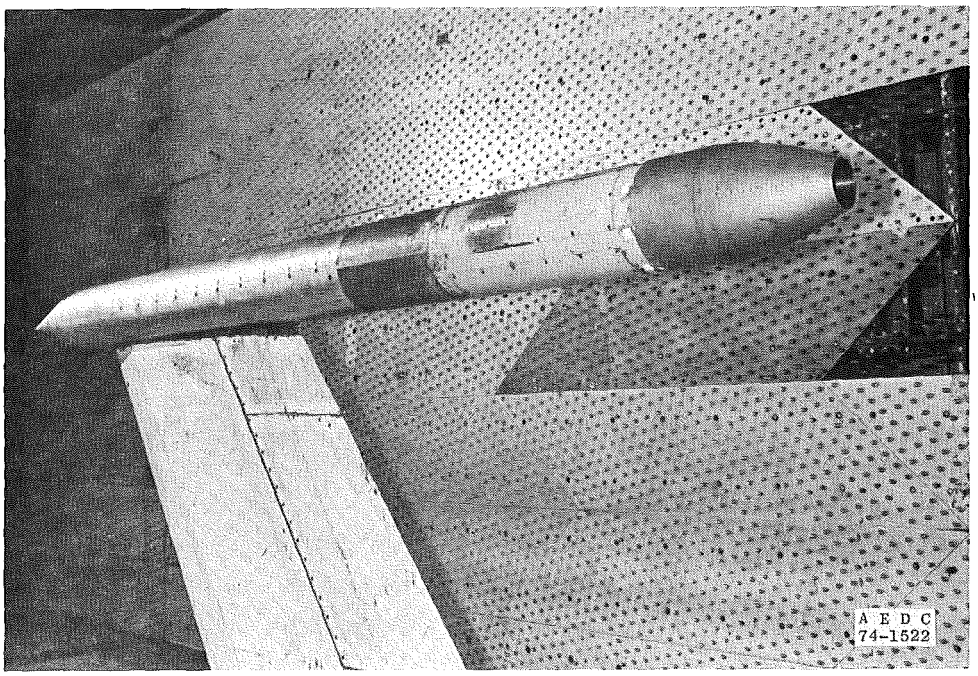

Figure 1. Full-size model installed in the AEDC Tunnel 16T, Phase I.

2.1.2 Lockheed-Georgia CFF

The CFF is a blowdown, transonic wind tunnel exhausting directly to the atmosphere, which is capable of being operated within the Mach number range from 0.2 to 1.25. The unit, which is described in detail in Ref. 4, is equipped with variable porosity test section walls similar to those in the AEDC Aerodynamic Wind Tunnel (4T) and are capable of having the porosity varied from zero to ten percent. The CFF test section has dimensions of 20 by 28 in. and is 72 in. in length. A maximum stagnation pressure of 175 psia allows operation within a Reynolds number range from 6 x 10^6 to 50 x 10^6 ft. A photograph of the 0.15-percent scale model installed in the CFF is shown in Fig. 2.

2.2 EXPERIMENTAL HARDWARE

The Phase II model utilized primarily in the Lockheed-Georgia CFF is a 0.15-scale model of the Phase I model which was tested in the AEDC Tunnel 16T. Both models were axisymmetric cone-cylinders with a 14-deg half-angle conical nose which was faired

into the cylindrical midsection. The models were supported in the test sections by struts which had a sweep angle of 31.8 deg aft. High-pressure air for jet plume simulation was ducted to the models through the strut. Both models had a boundary-layer trip located at an (L-X)/D of 1.217, measured from the cone vertex. The Phase I model trip consisted of 0.055-in.-diam steel spheres spotwelded to a trip ring at a circumferential spacing of four sphere diameters. The Phase II model boundary-layer trip consisted of 240 Grit sparsely distributed over a 0.1-in.-width band. Figure 3 presents the basic model dimensions for both models.

The Phase I model had an overall length of 146.63 in. and a diameter of 9.86 in., while the Phase II model had an overall length of 22.247 in. and a diameter of 1.54 in.

Three NAB configurations, defined by the AGARD Propulsion Energetics Panel (PEP)/ Fluid Dynamics Panel (FDP) Working Group on Nozzle Testing Techniques in Transonic Flow, were used during the Phase I investigation (Fig. 4). The configurations differed in the geometry of the external surfaces with mean closure angles of 10, 15, and 25 deg, respectively. The coordinates of the respective afterbodies as a function of X/D measured from the nozzle exit plane are included in Table 1. The Phase II model afterbody was a 0.15-scale model of the 15-deg Phase I afterbody configuration. A common sonic flow internal nozzle was used for each of the three Phase I configurations, with a scale model of the nozzle employed on the Phase II test article.

A limited amount of operation of the subscale model in the AEDC Tunnel 16T was conducted in an attempt to obtain data free of any tunnel wall interference effects. The Phase II model was positioned on the tunnel centerline using a strut support which was mounted on a sting support system. A photograph of this installation is presented in Fig. 5.

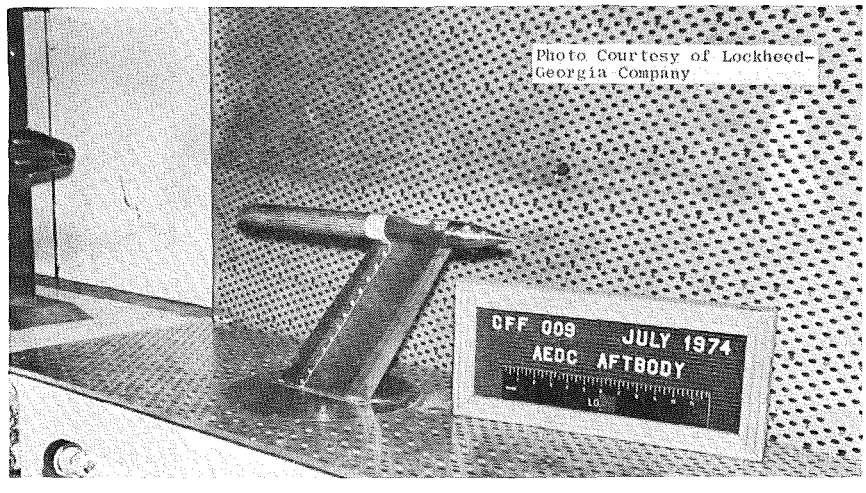

Figure 2. 0.15-scale model installed in the Lockheed-Georgia CFF, Phase II.

	Full Scale	Subscale
L	146.63	22.247
D	9.86	1.54
X_1	83.00	10.75
X_{ℓ}	96.00	14.0
S_1	35.30	4.43
S_2	50.90	5.86

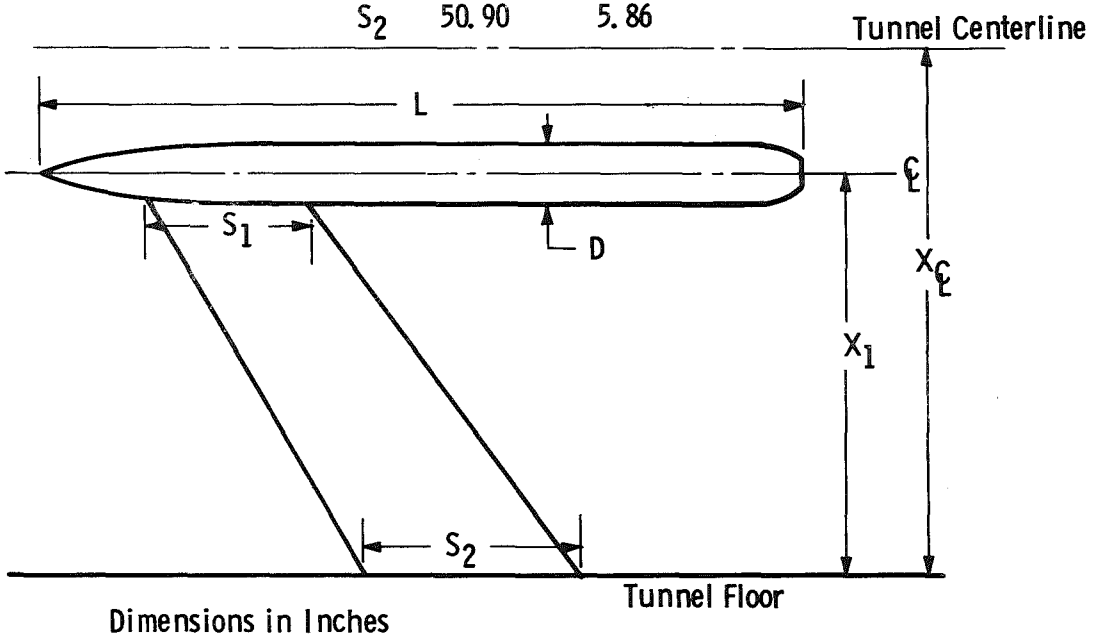

Figure 3. Basic dimensions of model.

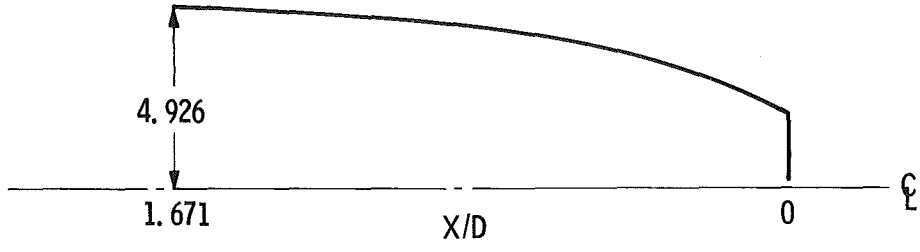

10-deg Afterbody

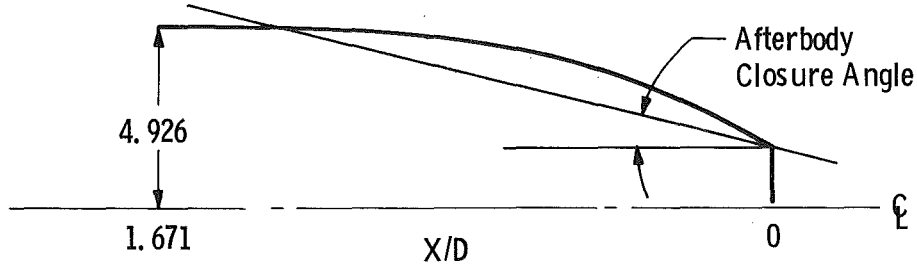

15-deg Afterbody

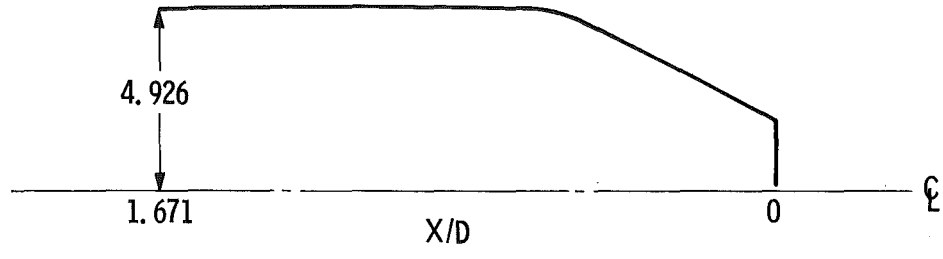

25-deg Afterbody

Figure 4. Nozzle afterbody configurations.

Table 1. Nozzle Afterbody External Coordinates

Configuration/Closure Angle, deg							
NAB, 10		NAB, 15		NAB, 25		Subscale, 15	
X/D	R	X/D	R	X/D	R	X/D	R
1.524	4.897	1.500	4.922	1.426	4.926	1.356	0.770
1.280	4.799	1.398	4.922	1.325	4.926	0.981	0.768
1.182	4.706	1.296	4.921	1.223	4.926	0.906	0.751
1.100	4.613	1.195	4.920	1.122	4.926	0.838	0.734
1.016	4.514	1.093	4.919	1.020	4.926	0.787	0.721
0.948	4.426	0.991	4.884	0.919	4.926	0.725	0.701
0.875	4.332	0.912	4.795	0.817	4.926	0.664	0.679
0.806	4.229	0.845	4.693	0.716	4.926	0.623	0.663
0.732	4.120	0.789	4.591	0.614	4.886	0.572	0.642
0.658	4.000	0.729	4.470	0.584	4.800	0.532	0.624
0.600	3.896	0.673	4.352	0.553	4.672	0.488	0.604
0.540	3.780	0.628	4.245	0.520	4.509	0.453	0.587
0.533	3.646	0.580	4.117	0.487	4.342	0.412	0.565
0.422	3.513	0.540	4.004	0.452	4.167	0.372	0.545
0.372	3.379	0.498	3.882	0.416	3.986	0.330	0.522
0.326	3.246	0.458	3.756	0.378	3.798	0.277	0.490
0.279	3.094	0.415	3.615	0.338	3.602	0.243	0.470
0.235	2.941	0.374	3.477	0.297	3.403	0.190	0.437
0.189	2.773	0.337	3.345	0.253	3.200		
0.141	2.584	0.286	3.160	0.205	2.982		
0.083	2.342	0.255	3.042	0.154	2.747		
0.028	2.134	0.192	2.795	0.098	2.485		
		0.142	2.584	0.035	2.198		
		0.092	2.364				
		0.035	2.144				

Notes: 1. X/D measured from nozzle exit plane.
2. R, dimensions in in.

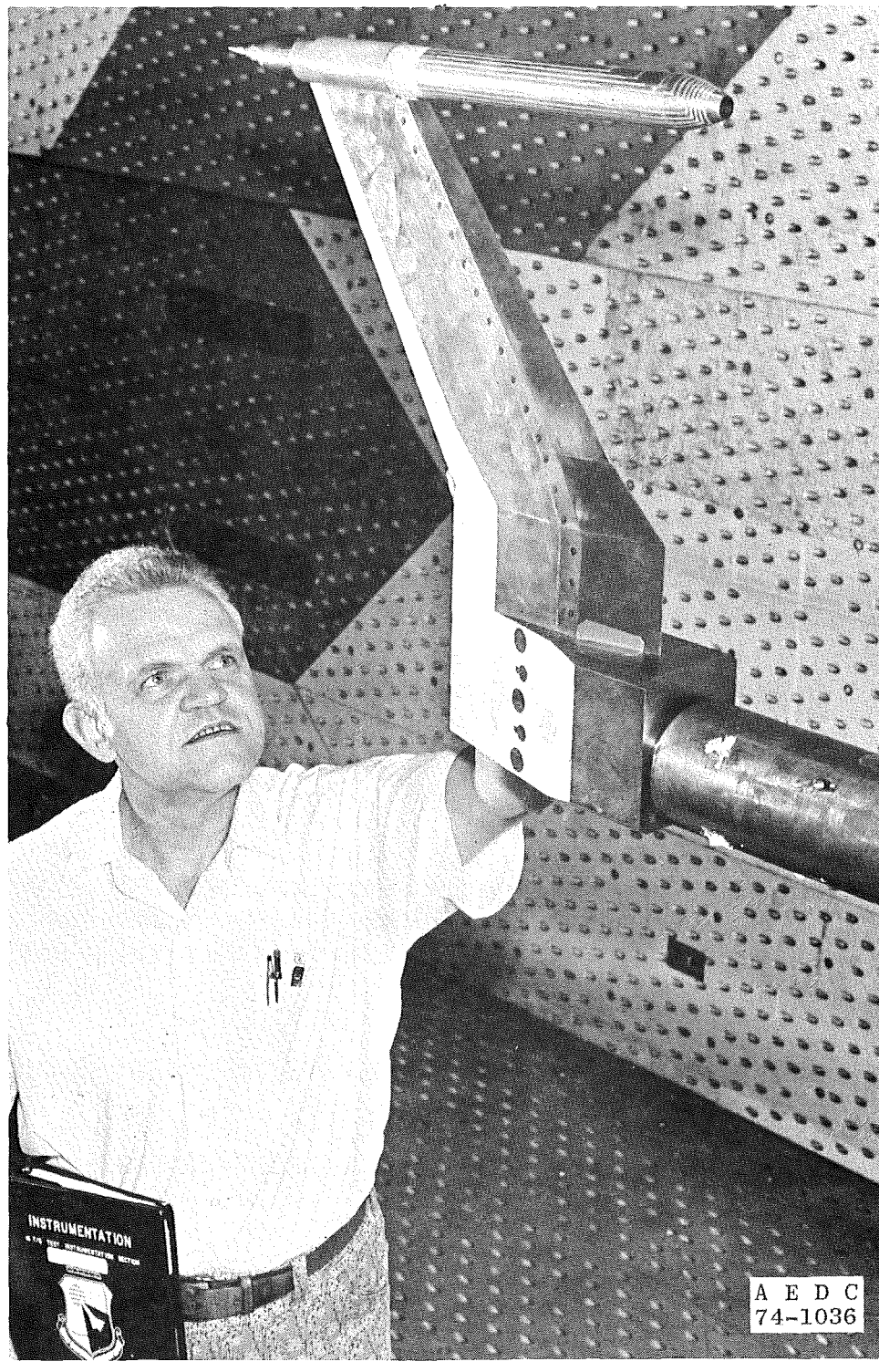

Figure 5. 0.15-scale model installed in the AEDC Tunnel 16T, Phase II.

2.3 INSTRUMENTATION

The primary instrumentation for both phases of this investigation measured external model static pressures along the top surface (Table 2). These pressures were then integrated to determine pressure drag force. In addition to the surface pressure measurements, internal model pressures were measured with a total-pressure rake in Phase I (Fig. 6a) and a total-pressure probe in Phase II (Fig. 6b). Model mass flow rates for both phases were measured with critical flow venturis.

In the AEDC Tunnel 16T, a precision pressure balance pressure measuring system was used with uncertainties of ±1.854 and ±2.34 psf at Reynolds numbers of 11.0 and 27.5 x 10^6, respectively. Accuracies of ±0.93 percent on model mass flow rate were obtained with the critical flow venturis. In the Lockheed-Georgia CFF, two Scanivalves, Inc. pressure scanners were used, in conjunction with Statham Instruments bidirectional differential pressure transducers which had a ±50-psi pressure range and an accuracy of 0.25 percent, to measure the external pressure distributions.

The number of pressure taps was different for each afterbody (Table 2). Twenty-two, 25, and 23 taps were used on the 10-, 15-, and 25-deg afterbodies, respectively. The Phase II subscale 15-deg afterbody had 19 pressure taps. The accuracy of the integrated pressure drag is related to the number and location of the pressure taps and is, therefore, more accurate for the full-scale model than for the subscale model.

3.0 PROCEDURES

3.1 EXPERIMENTAL PROCEDURES

The experimental investigation was divided into two phases which were distinguished by two different tunnels and two models (Section 2.0). The operational procedures used to obtain the data were different for the two tunnels and will be enumerated separately.

AEDC Tunnel 16T, Phase I and II

1. Wind tunnel Mach number and Reynolds number conditions were established, and jet-off data were obtained.

2. Airflow to simulate the exhaust plume was established through the model, and a series of nozzle pressure ratios were set. Data were obtained at each ratio.

Mach number and Reynolds numbers were primary variables, and data were obtained over the range of nozzle pressure ratios for the Mach number and Reynolds number conditions listed in Table 3. At each pressure ratio condition, a minimum of three data points were taken to ensure that stable conditions on the model existed.

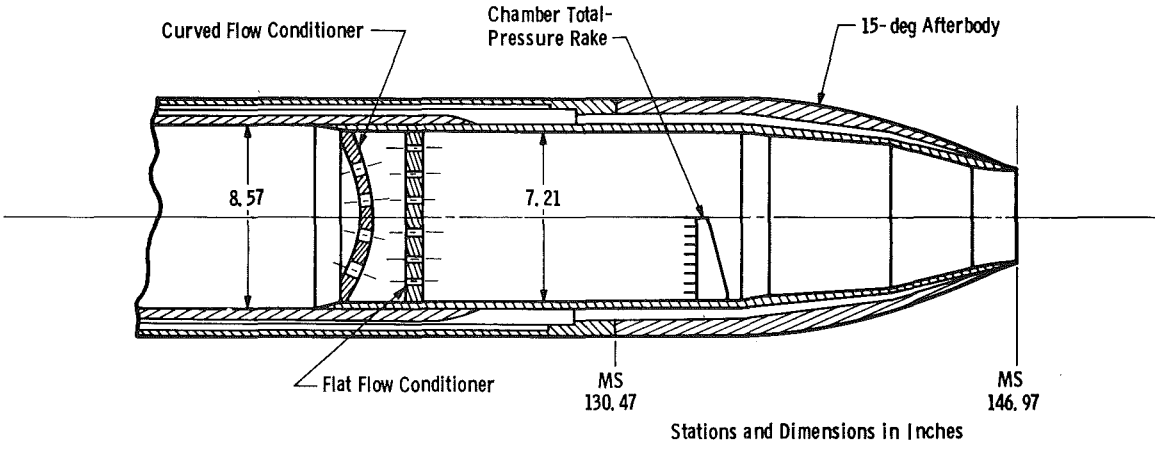

a. Full-size model (Phase I)

Figure 6. Flow channel instrumentation and dimensions.

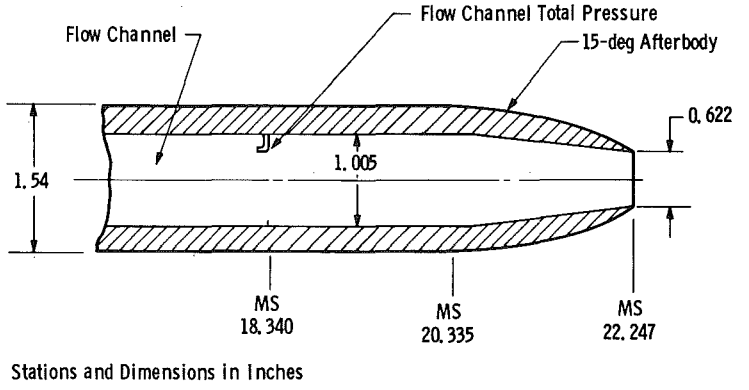

b. 0.15-scale model (Phase II)

Figure 6. Concluded.

Table 2. Nozzle Afterbody Surface Pressure Tap Locations

Configuration/Closure Angle, deg							
NAB, 10		NAB, 15		NAB, 25		Subscale, 15	
Pxxx	X/D	Pxxx	X/D	Pxxx	X/D	Pxx	X/D
P401	1.519	P401	1.500	P401	1.424	P4	1.364
P402	1.276	P402	1.393	P402	1.323	P5	1.088
P403	1.179	P403	1.291	P403	1.221	P6	0.987
P404	1.097	P404	1.190	P404	1.120	P7	0.908
P405	1.013	P405	1.088	P405	1.018	P8	0.842
P406	0.945	P406	0.986	P406	0.917	P9	0.786
P407	0.872	P407	0.907	P407	0.815	P10	0.726
P408	0.803	P408	0.841	P408	0.714	P11	0.671
P409	0.730	P409	0.785	P409	0.612	P12	0.625
P410	0.656	P410	0.724	P410	0.582	P13	0.578
P411	0.598	P411	0.669	P411	0.551	P14	0.538
P412	0.538	P412	0.624	P412	0.518	P15	0.497
P413	0.476	P413	0.576	P413	0.485	P16	0.456
P414	0.421	P414	0.536	P414	0.450	P17	0.413
P415	0.370	P415	0.494	P415	0.414	P18	0.373
P416	0.324	P416	0.454	P416	0.376	P19	0.335
P417	0.277	P417	0.411	P417	0.337	P20	0.285
P418	0.233	P418	0.370	P418	0.295	P21	0.253
P419	0.188	P419	0.332	P419	0.251	P22	0.190
P420	0.140	P420	0.282	P420	0.203		
P421	0.082	P421	0.251	P421	0.152		
P422	0.027	P422	0.187	P422	0.096		
		P423	0.129	P423	0.033		
		P424	0.088				
		P425	0.031				

Notes: 1. X/D measured from nozzle exit plane.
2. Pxxx and Pxx - Pressure tap identification number.

Table 3. Test Matrix of the Phase I Investigation

Afterbody Config	Re x 10^{-6}	M_∞					
		0.6	0.8	0.9	0.95	1.1	1.5
10-deg	12.2	X	X	X	X	X	X
	21.4	X	X	X	X	X	X
	30.6	X	X	X	X	X	X
	42.8	---	---	---	---	---	X
	61.2	X	X	X	X	---	---
15-deg	12.2	X	X	X	X	X	X
	21.4	X	X	X	X	X	X
	30.6	X	X	X	X	X	X
	42.8	---	---	---	---	---	X
	61.2	X	X	X	X	X	---
25-deg	12.2	---	---	X	X	X	X
	21.4	X	X	X	X	X	X
	30.6	X	X	X	X	X	X
	42.8	---	---	---	---	---	X
	61.2	X	X	X	X	X	---

Lockheed-Georgia CFF, Phase II

The Lockheed-Georgia CFF is a blowdown tunnel and, therefore, operates in a different manner than does the continuous flow AEDC Tunnel 16T.

1. The desired Mach number is obtained by positioning the ejector flaps according to a prescribed schedule which was determined during tunnel calibration.

2. The Reynolds number is established by setting the total pressure in the tunnel settling chamber by positioning a sleeve-type control valve.

3. Flow was established through the model to yield the desired nozzle pressure ratio.

4. Tunnel flow was established, and the forward pressure on the model was monitored electronically. When the pressure on the model had stabilized, the data system was scanned electronically and tunnel flow was then terminated.

3.2 DATA REDUCTION PROCEDURES

The basic equation used to calculate the pressure drag on the nozzle aftebody is given as

$$C_{D_p} = \frac{\pi}{2AREF} \sum_{L=x}^{n} (C_{pi} + C_{pi+1})(R_i^2 - R_{i+1}^2) \quad (1)$$

where AREF is the reference area of the respective models calculated from the relationship

$$AREF = \frac{\pi}{4} D^2 \quad (2)$$

where D is the maximum body diameter. In Eq. (1), i refers to the conditions at the local static pressure taps and the summation is initiated at the x location of the forwardmost pressure tap on the afterbody. R is the local body radius. C_p in Eq. (1) is the local pressure coefficient calculated from the local measured static pressure using the following relationship

$$C_p = \frac{p_i - p_\infty}{q_\infty} \quad (3)$$

where p_∞ and q_∞ are the local free-stream static pressure and dynamic pressure, respectively.

The relationship in Eq. (1), with the appropriate inputs, was used to calculate the afterbody drag coefficient for all three NAB configurations of the Phase I model, as well as for the Phase II model.

4.0 EXPERIMENTAL RESULTS

4.1 GENERAL

The investigation covered a test matrix shown in Tables 3 and 4. Table 3 lists the test conditions investigated during Phase I with the full-size model in Tunnel 16T. The effect of Reynolds number was measured on three afterbodies with closure angles of 10, 15, and 25 deg (Fig. 4). In the Phase II experiments, conducted in the Lockheed-Georgia CFF, an afterbody with a 15-deg closure angle was investigated at the conditions listed in Table 4a. The 0.15-scale Phase II model was also operated in Tunnel 16T at the conditions listed in Table 4b.

Table 4. Test Matrix of the Phase II Investigation

a. CFF Investigation

Wall Porosity, percent	Re x 10^{-6}	M_∞				
		0.6	0.8	0.9	0.95	1.1
2	11.0	x	x	x	x	x
	27.5	x	x	x	x	x
	55.0	x	x	x	x	x
	91.7	x	x	x	x	x
4	11.0	x	x	x	x	x
	27.5	x	x	x	x	x
	55.0	x	x	x	x	x
	91.7	x	x	x	x	x
6	11.0	x	x	x	x	x
	27.5	x	x	x	x	x
	55.0	x	x	x	x	x
	91.7	x	x	x	x	x

b. Tunnel 16T Investigation

Wall Porosity, percent	Re x 10^{-6}	M_∞				
		0.6	0.8	0.9	0.95	1.1
6	1.8	x	x	x	x	---
	2.8	x	---	---	---	---
	3.1	---	---	x	x	---
	4.6	x	x	x	x	x
	6.9	---	x	x	---	---
	8.6	---	---	x	---	---
	9.2	x	x	x	x	---
	11.0	x	---	---	---	---

The afterbody pressure drag coefficient (C_{D_p}) was chosen as the primary parameter to determine the effects of Reynolds number and tunnel wall porosity variations on nozzle afterbody performance. This coefficient was determined from an integration of the pressure measurements along the model afterbody external surfaces. A comparison of the pressure distributions obtained for the Phase I and Phase II models with 15-deg closure angle afterbodies at Mach numbers 0.6 and 0.9 is shown in Figs. 7a and b at a Reynolds number of 30 x 10^6. The pressure distributions measured on each model are similar for both of the Mach numbers shown. The expansion along the afterbody of the Phase II model, however, did not attain the same minimum value of C_p as the Phase I model for either of the Mach numbers. At Mach number 0.6 the expansion and recompression occurred further upstream on the Phase I model than it did on the Phase II model, although the rate of recompression was the same. At Mach number 0.9, the recompression occurred at the same axial station for both models; however, the expansion began further upstream on the Phase I model. These differences in expansion, recompression, and the minimum value obtained on the expansion strongly affect the afterbody pressure drag coefficient as can be seen from the tabulated values included in Figs. 7a and b. The differences in the expansion-recompression behavior might be caused either by differences in the afterbody geometry which could occur during manufacturing or small differences in tunnel operating characteristics.

The pressure distributions shown in Figs. 7a and b show that pressures were measured farther downstream on the Phase I model than on the Phase II model. In order to make a direct comparison between the two experimental programs it was necessary to truncate the integration at an X/D of 0.225, measured upstream of the nozzle exit. This truncation results in a higher afterbody pressure drag coefficient than actually exists, because a portion of the recompression is eliminated from consideration. However, the resulting coefficients should be directly comparable for both models.

4.2 COMPARISON OF C_{D_p} AS A FUNCTION OF NPR FOR PHASE I AND II MODELS

The pressure distributions were measured and C_{D_p} calculated from those measurements at each of the Mach numbers and Reynolds numbers listed in Tables 3 and 4 with nozzle pressure ratio (NPR) as a variable. (Mach number 1.5 data obtained during Phase I are not included here but can be found in Ref. 1.) Figure 8 presents a comparison of C_{D_p} for the Phase I and Phase II models as a function of NPR for each of the five Mach numbers investigated at Reynolds numbers of approximately 11, 30, and 60 x 10^6. The drag coefficients for both the Phase I and Phase II models display the characteristic behavior of an isolated nozzle afterbody with varying NPR. The characteristic behavior of C_{D_p} with increasing NPR is to initially rise to a maximum value followed by a decrease with further increases in NPR. The NPR at which the maximum value of C_{D_p} is reached is Mach number dependent. (The mechanisms which govern this characteristic behavior are discussed in Ref. 5 and will not be repeated here.) The general

shape of the relationship of C_{D_p} with NPR is similar for both Phase I and Phase II models for both the Reynolds numbers shown in Fig. 8. However, the absolute levels of C_{D_p} differ between the two models. At Mach 0.6 the Phase I (Tunnel 16T) drag coefficient was lower than that determined from the subscale model in the Lockheed tunnel. At Mach 0.8, however, the relative values were reversed, with the C_{D_p} determined in Tunnel 16T on the full-scale model being larger than the C_{D_p} determined on the Phase II model. At the succeedingly higher Mach numbers (0.9, 0.95, and 1.1), the difference in C_{D_p} for the two models increased with the large model producing the highest drag coefficient values. This discrepancy in absolute value is not understood.

To show the effect of Reynolds number on C_{D_p}, a single NPR of 3.0 will be used throughout the remainder of data presentations. An NPR of 3.0 was chosen because it represents approximately the maximum drag on the afterbody (Fig. 8).

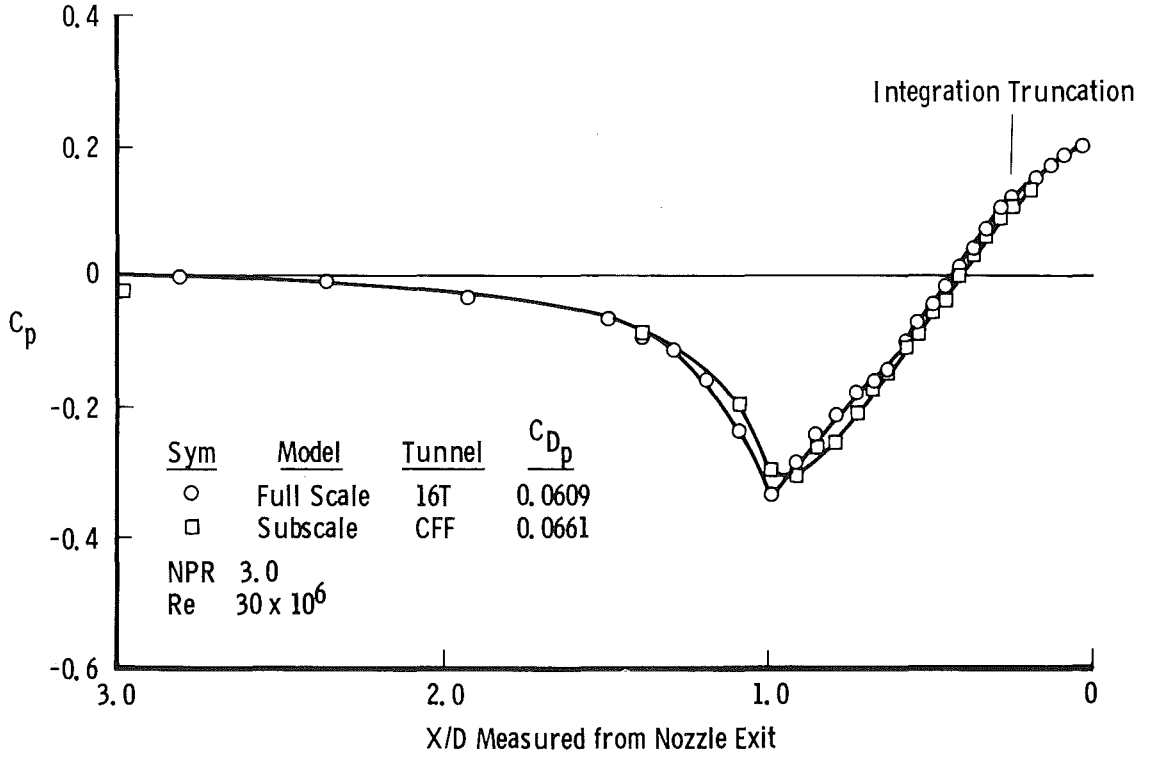

a. $M_\infty = 0.6$

Figure 7. Comparison of the static pressure distributions measured on the Phase I and Phase II models at a nozzle pressure ratio of 3.0.

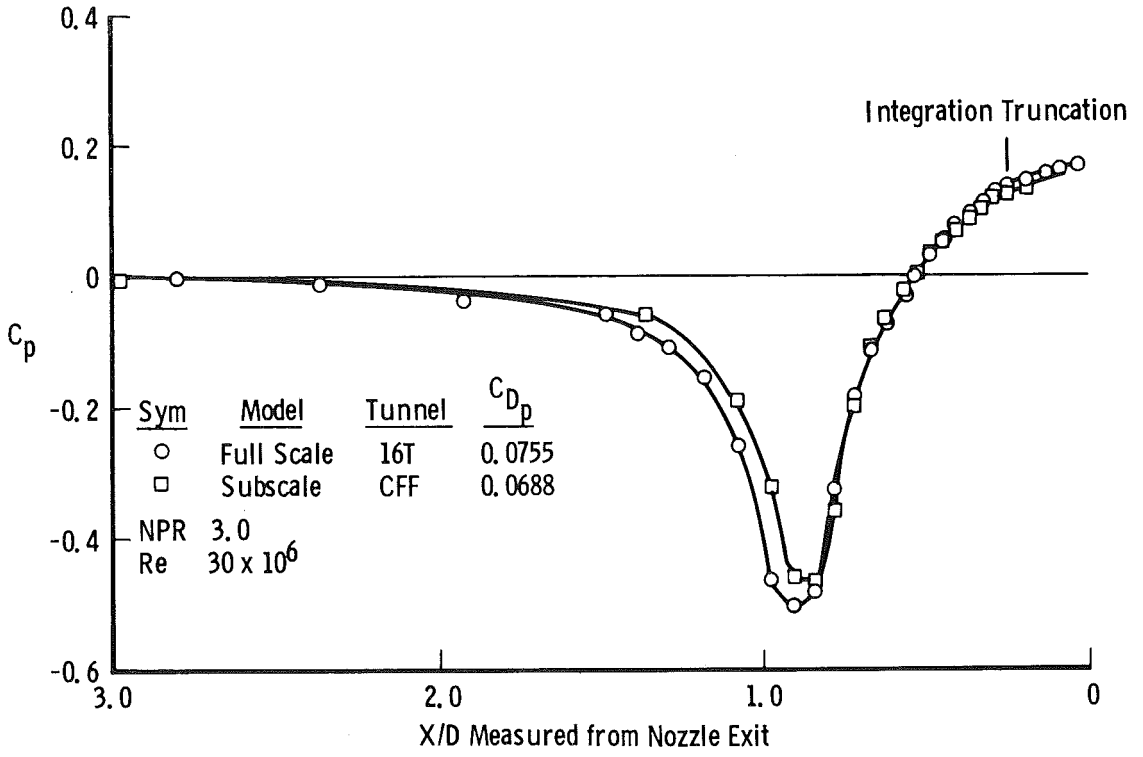

b. $M_\infty = 0.9$

Figure 7. Concluded.

4.3 COMPARISON OF REYNOLDS NUMBER EFFECT ON PHASE I AND II MODELS

A comparison of the effect of Reynolds number on the Phase I 15-deg afterbody and the Phase II model is presented in Figs. 9a through e for five Mach numbers. Over a range of Reynolds numbers from 10 x 10^6 to 90 x 10^6, the behavior of the pressure drag coefficient (C_{D_p}) was Mach number dependent for both models. At Mach number 0.6 and 0.8, C_{D_p} was essentially constant with Reynolds number over the range investigated. At Mach number 0.9, 0.95, and 1.1, C_{D_p} increased with increasing Reynolds number. Both the Phase I and Phase II data displayed similar trends with increasing Reynolds numbers at all Mach numbers. The Phase II model was also tested over a limited range of Reynolds numbers in the AEDC Tunnel 16T in an attempt to obtain NAB performance data that were free from tunnel wall effects. The model was supported on its strut which was mounted on a sting support system (Fig. 5). The results of this part of the investigation are included in Figs. 9a through e for comparison with the Phase I and Phase II CFF results. At subsonic Mach numbers (0.6, 0.8, and 0.9), the "interference-free" drag coefficient agreed closely with the drag coefficient obtained on the Phase I investigation; however, at Mach numbers 0.95 and 1.1 higher drag levels were

calculated for the Phase II model in Tunnel 16T than either the full-scale Phase I model in Tunnel 16T or the Phase II model in the Lockheed-Georgia CFF. Because of the size of the sting on which the model was mounted, which provided an unfavorable area distribution, the C_{D_p} results on the Phase II model in Tunnel 16T are suspect. An analysis of the subscale mounting arrangement in Tunnel 16T (Ref. 6) was conducted using the Krupp and Murman transonic computational technique. An equivalent body of revolution was derived from the area distribution of the sting-strut combination, and the pressure distribution (at a distance away from this equivalent body corresponding to where the model would be located) was then calculated. Reference 6 shows that for Mach number 0.95 the equivalent body produces an expansion upstream of the nozzle afterbody which affects the pressure distribution.

4.4 EFFECT OF REYNOLDS NUMBER ON PRESSURE DISTRIBUTION

The drag coefficient, as previously stated, is determined from an integration of the measured pressure distribution on the afterbody surface. A comparison of the static pressure distribution at a Reynolds number of approximately 10×10^6 and 90×10^6 for the Phase II model at a pressure ratio of 3.0 is presented in Figs. 10a and b for Mach number 0.6 and 0.9, respectively. At Mach number 0.6, the pressure distribution is essentially the same at both Reynolds numbers and will give approximately the same C_{D_p} when integrated. However, at Mach number 0.90 the pressure distribution for the higher Reynolds number reached a lower C_p before recompression and had a stronger recompression over the remainder of the afterbody. This behavior, which was reported in Ref. 7, is typical for isolated NAB configurations. When these distributions are integrated over the afterbody, the lower C_p (resulting from increased expansion and the stronger recompression of the higher Reynolds number pressure distribution) produces compensating effects, with the result indicating the reason for the weak dependency of C_{D_p} on Reynolds number variations.

4.5 INFLUENCE OF NAB GEOMETRY ON REYNOLDS NUMBER EFFECTS

The effect of Reynolds number on three afterbody configurations with closure angles of 10, 15, and 25 deg is shown in Figs. 11a through e. It should be emphasized that the pressures along the entire afterbody surface were integrated to determine the C_{D_p}'s presented in these figures. For the 10- and 15-deg afterbodies, the effect of Reynolds number on C_{D_p} was similar, with the 10-deg afterbody showing the smallest effect. The C_{D_p} of the 10-deg afterbody remained more nearly constant with varying Mach number than did the C_{D_p} calculated for the 15-deg afterbody. The behavior of the 25-deg afterbody was somewhat random in nature with varying Reynolds number and Mach number. Schlieren photographs show that the afterbody with the steep, 25-deg closure angle operated in a separated condition at all Mach numbers investigated. This separation accounts for the high drag level and the different behavior with Reynolds number and Mach number variations.

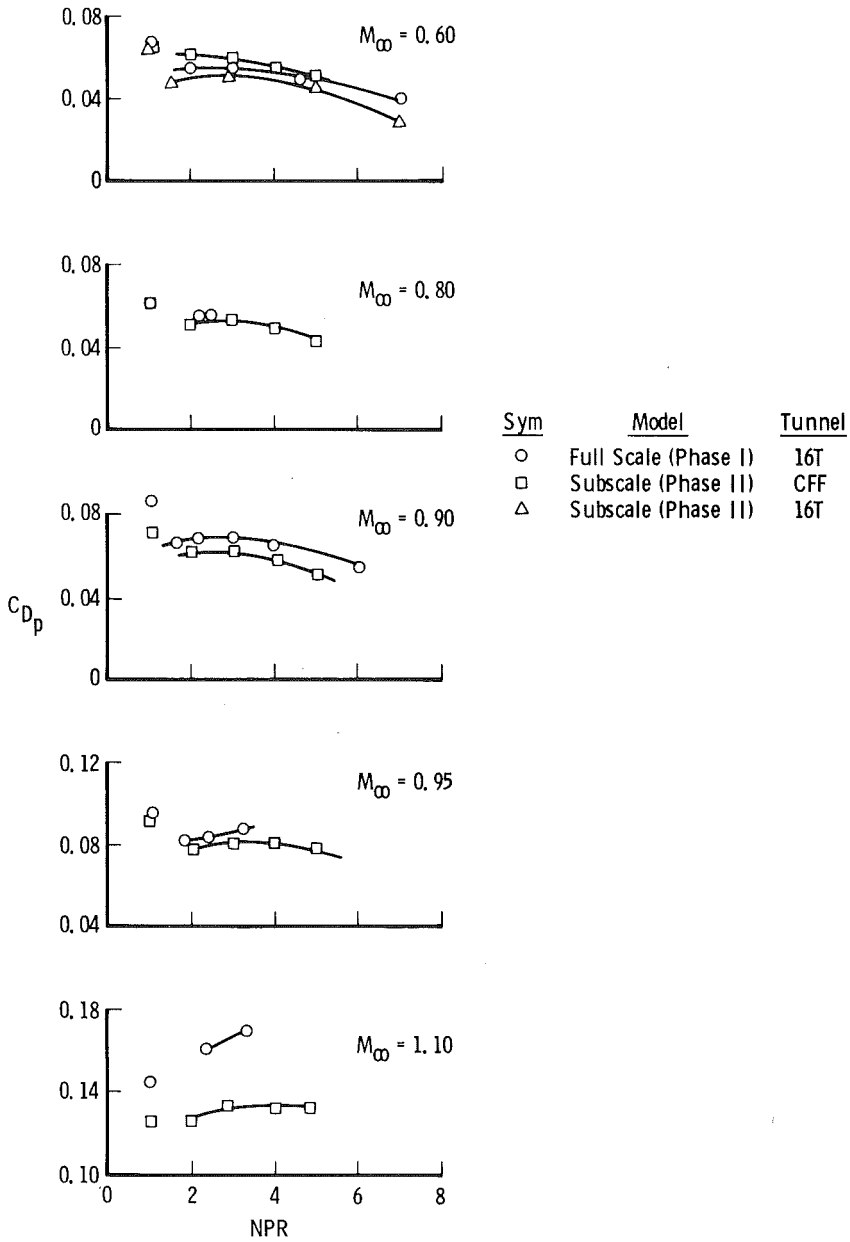

a. Re = 11 x 10^6

Figure 8. Comparison of the drag coefficient as a function of nozzle pressure ratio for the Phase I and Phase II models at three Reynolds numbers.

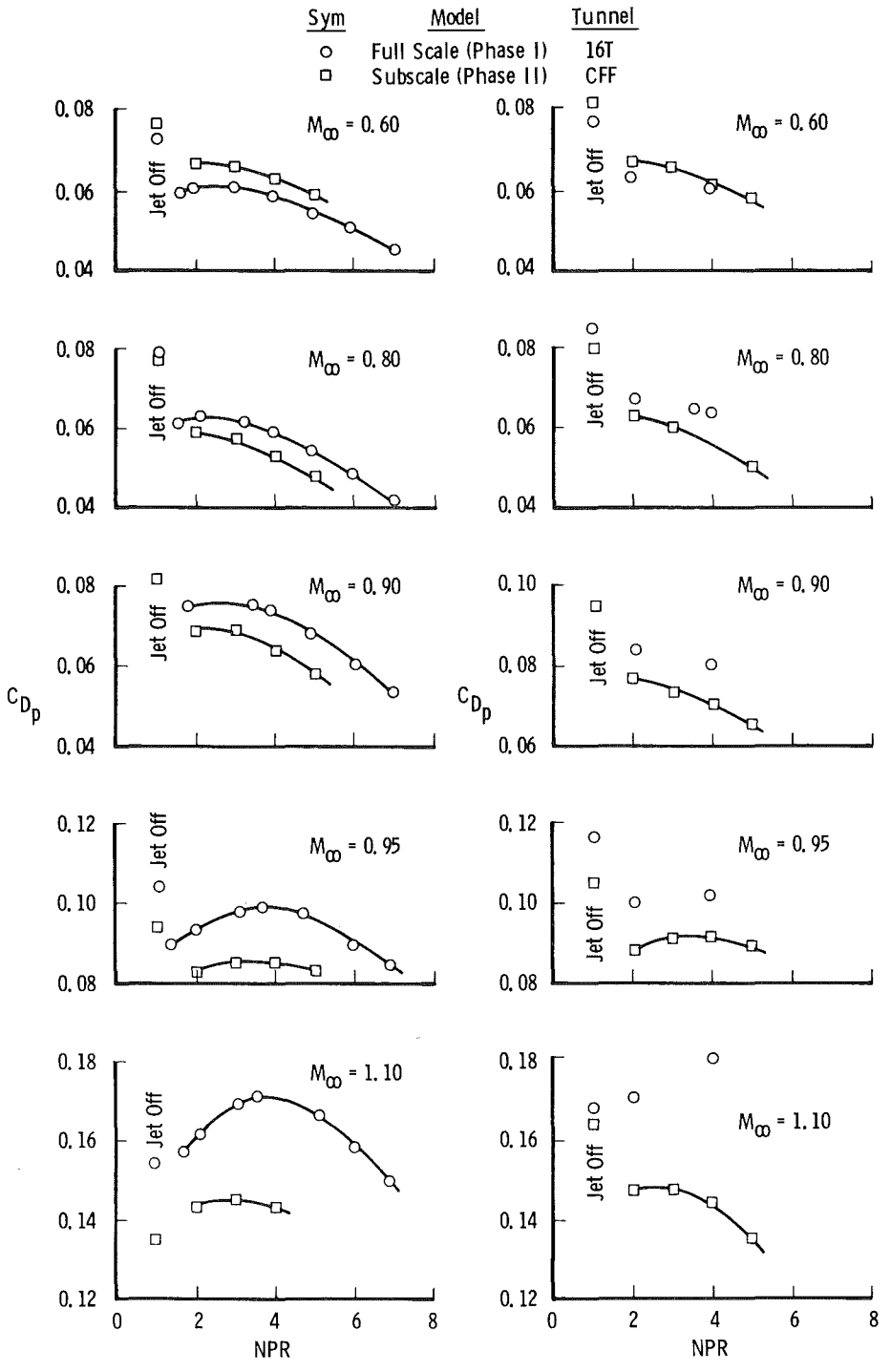

b. Re = 30 x 10^6

c. Re = 60 x 10^6

Figure 8. Concluded.

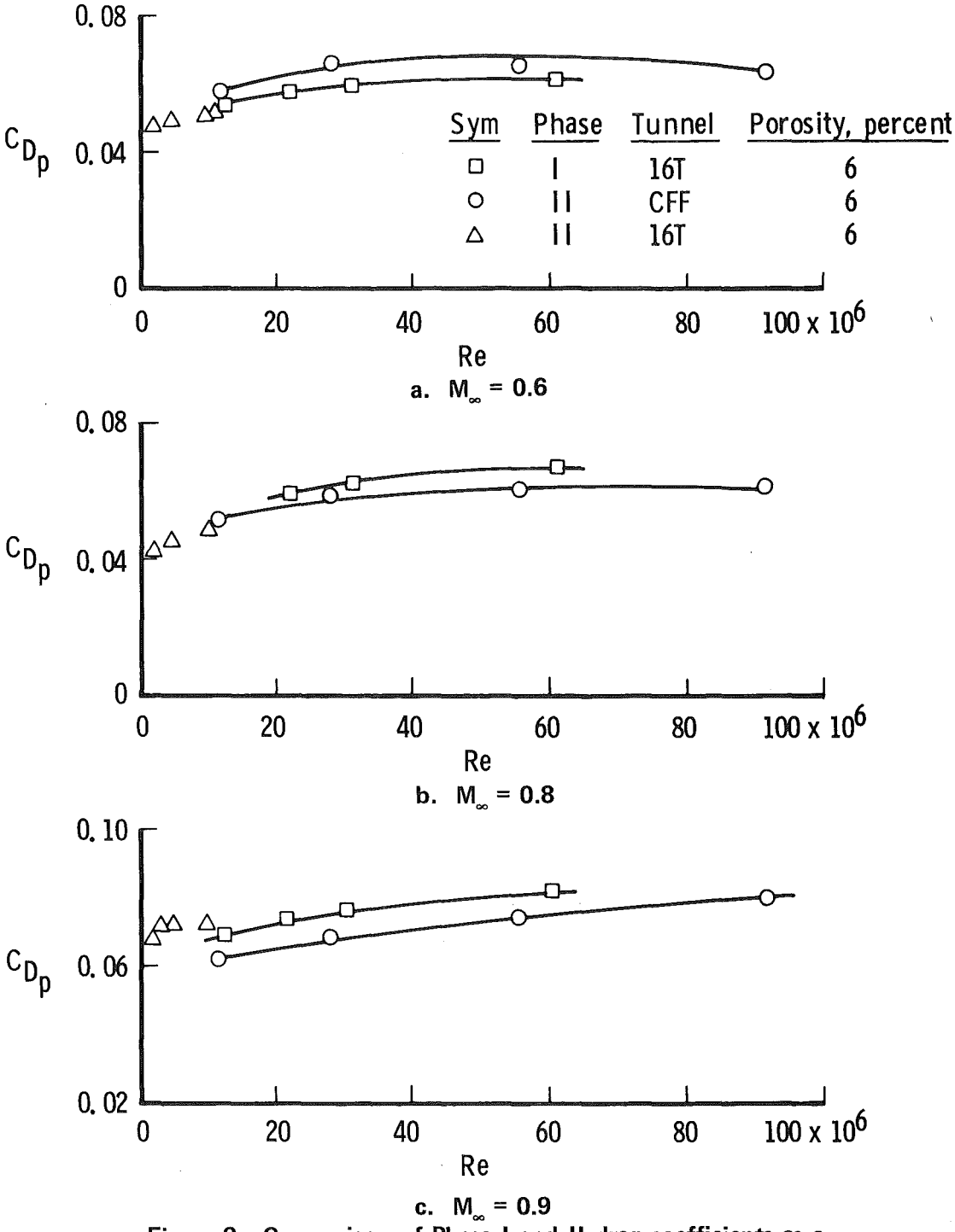

Figure 9. Comparison of Phase I and II drag coefficients as a function of Reynolds number at a nozzle pressure ratio of 3.0.

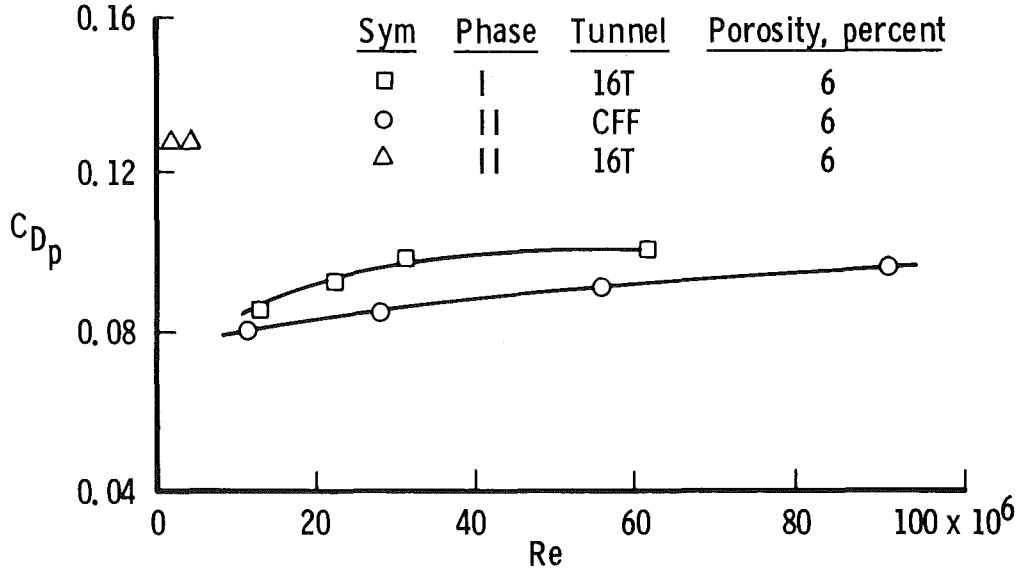

d. $M_\infty = 0.95$

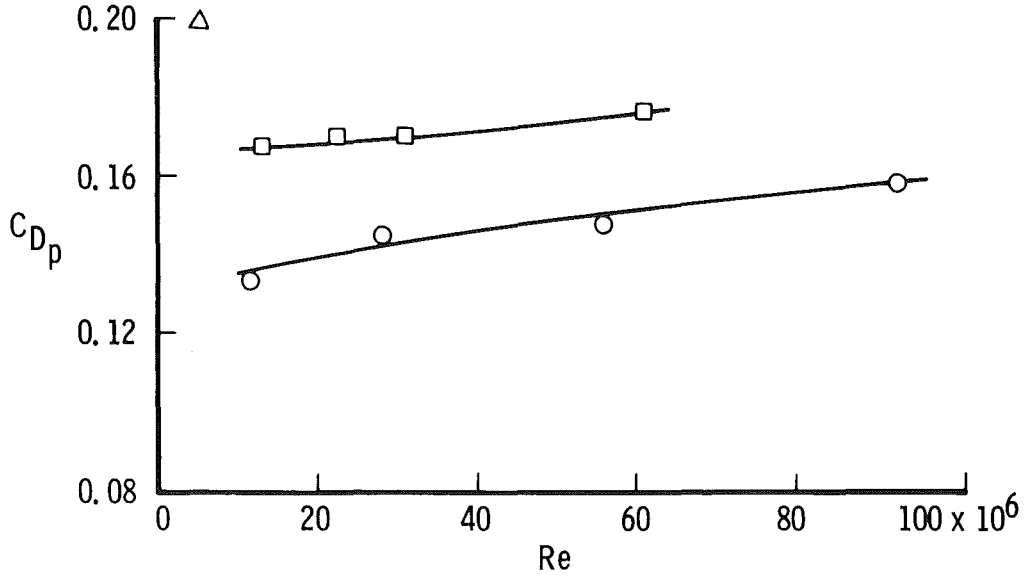

e. $M_\infty = 1.1$

Figure 9. Concluded.

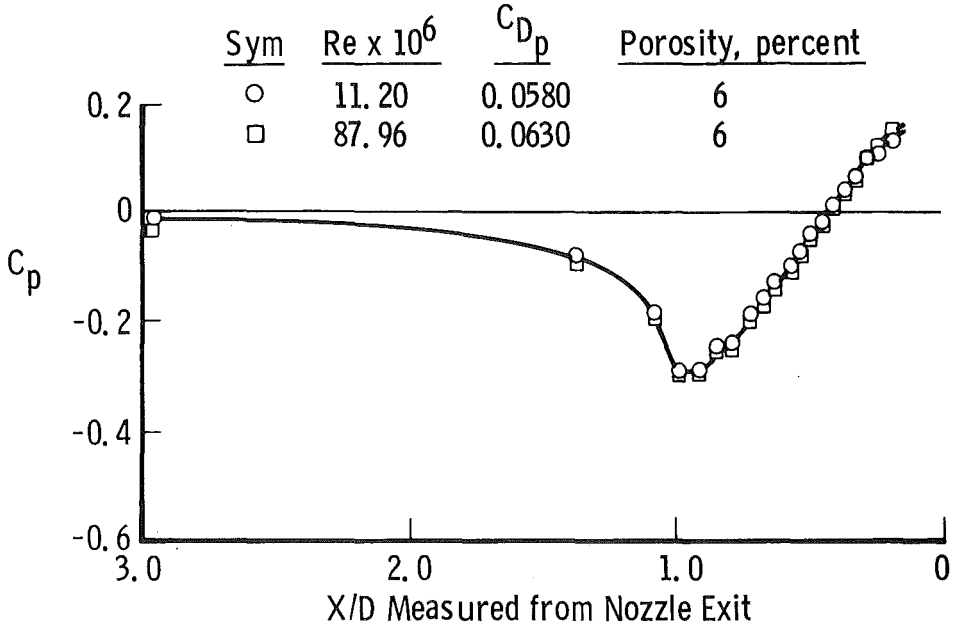

a. $M_\infty = 0.6$

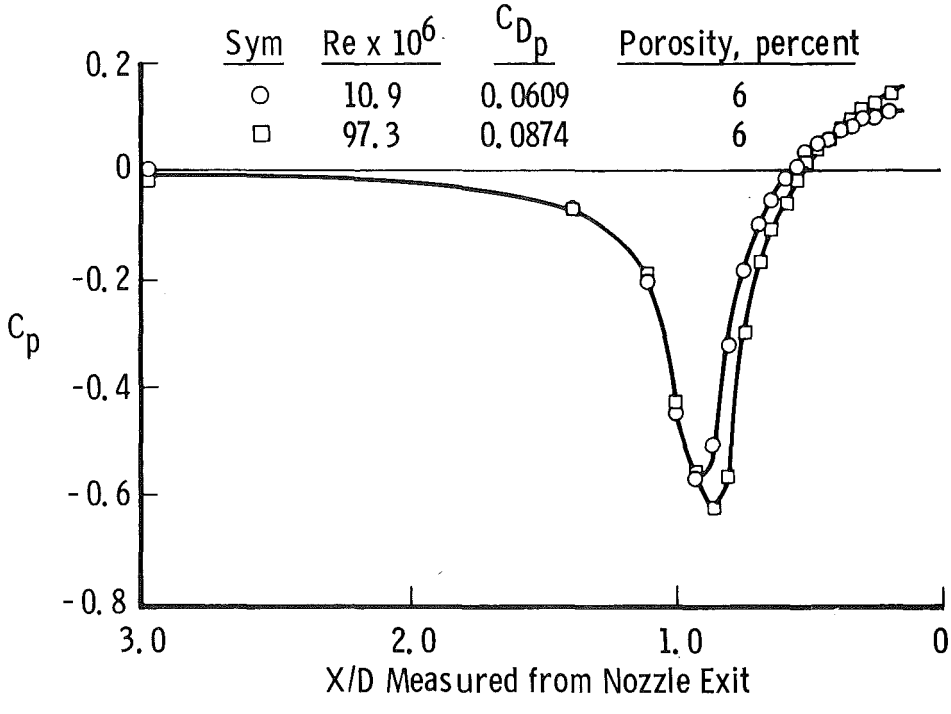

b. $M_\infty = 0.9$

Figure 10. Afterbody static pressure distribution for two Reynolds numbers, Phase II, CFF.

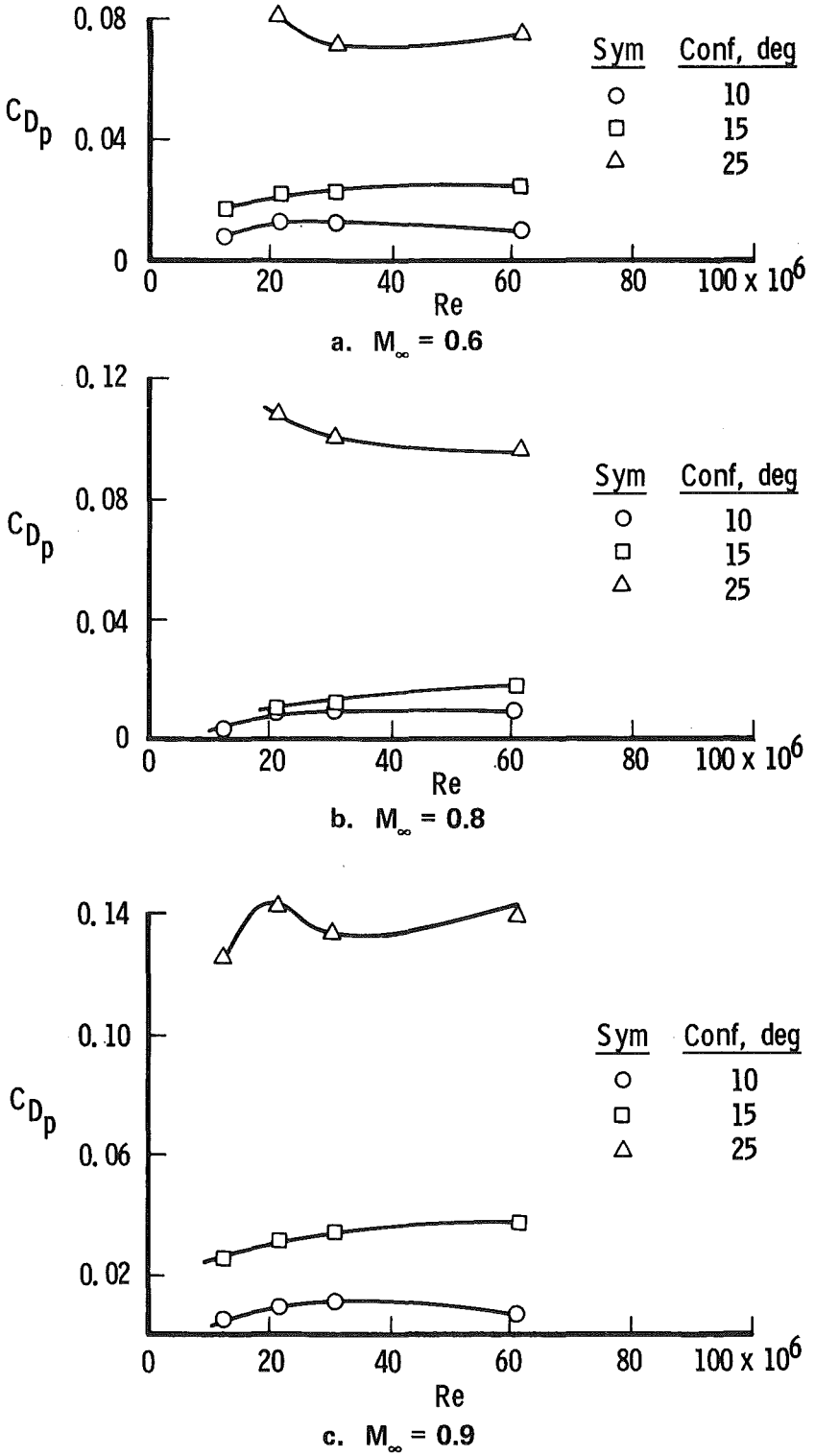

Figure 11. Effect of Reynolds number on afterbody drag coefficient for three afterbody configurations, Phase I.

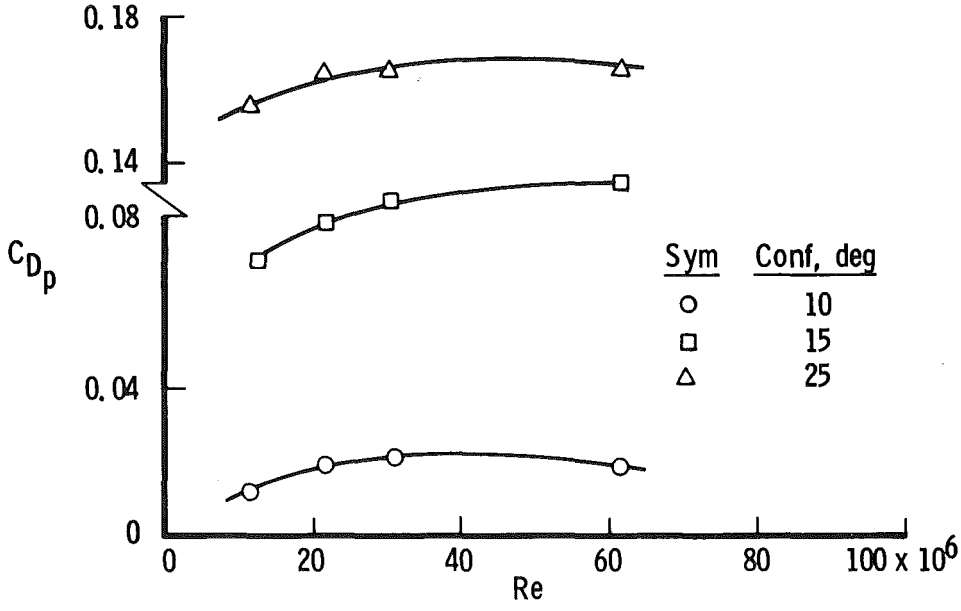

d. M_∞ = 0.95

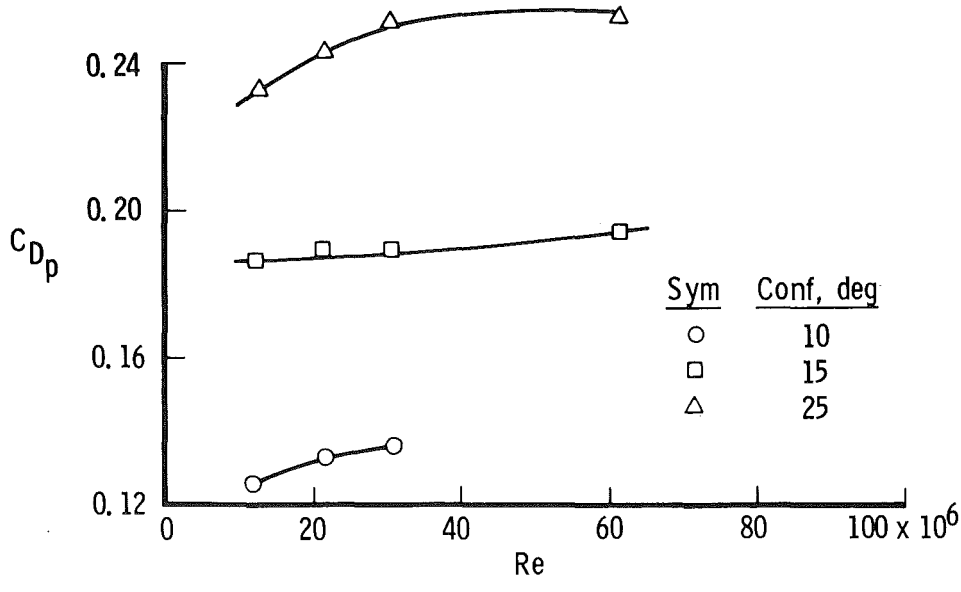

e. M_∞ = 1.1

Figure 11. Concluded.

4.6 INFLUENCE OF VARIABLE TUNNEL WALL POROSITY ON C_{D_p}

As a part of the Phase II NAB experimental program, studies of the effects of tunnel wall porosity on afterbody drag coefficient were investigated. The C_{D_p}'s were determined over the Mach number and Reynolds number range (Table 4) for values of wall porosities of two, four, and six percent. Figure 12 presents C_{D_p} as a function of Reynolds number at the five Mach numbers investigated with the porosities identified. The Phase I data are shown for comparison. The effect of porosity on C_{D_p} increased with increasing Mach number, ranging from essentially no effect at Mach 0.6 to a large effect at Mach number 1.1. From Fig. 12 the Phase II drag coefficient for the various porosities can be seen to bracket the drag coefficient obtained on the full-scale model in Tunnel 16T at a constant porosity of six percent. This indicates that a portion of the difference between the absolute level of the Phase I and Phase II data could be retrieved in the Lockheed-Georgia CFF by varying porosity at each Mach number until the best agreement is achieved. Figure 13, cross-plotted from Figs. 12a through e, presents C_{D_p} as a function of porosity taken at a constant Reynolds number of 50 x 10^6 for the five Mach numbers tested. At Mach number 0.6, varying porosity from two to six percent had no effect on C_{D_p}. At Mach number 0.8, C_{D_p} at porosities of six and four percent was constant, whereas C_{D_p} at a porosity of two percent was higher. The C_{D_p} increased with decreasing porosity at Mach numbers 0.8, 0.95, and 1.1.

4.7 COMPARISON OF EXPERIMENTAL RESULTS WITH NUMERICAL PREDICTIONS

An extensive effort is being conducted at the AEDC to develop the capability of numerically predicting the performance of nozzle afterbody configurations. Using existing computer codes and modifying these to address the particular problem area, much progress toward a workable procedure has been made. The effort is discussed in detail in Ref. 1 and will not be repeated here. However, using the coordinates of the Phase II model, predictions of the pressure distribution over the NAB at a Mach number of 0.6 and Reynolds numbers of 11, 28, 56, and 92 x 10^6 were made using this numerical technique. (The effect of Reynolds number is introduced into the numerical technique through the effect of Reynolds number on boundary-layer displacement thickness.) A comparison of the numerical predictions with experimental results is shown in Figs. 14a and b for Reynolds numbers of 11 x 10^6 and 92 x 10^6. The numerical prediction agrees closely with the experimental results in the expansion region of the flow. However, the recompression region is steeper for the numerical prediction than for the experimental results. Afterbody drag coefficient was determined, by pressure integration, for the numerical prediction and compared to the experimental results in Fig. 15. The trend with increasing Reynolds number is the same for both the numerical solution and the experimental data. The absolute level of drag coefficient, however, is lower for the numerical technique because the recompression on the afterbody is overpredicted.

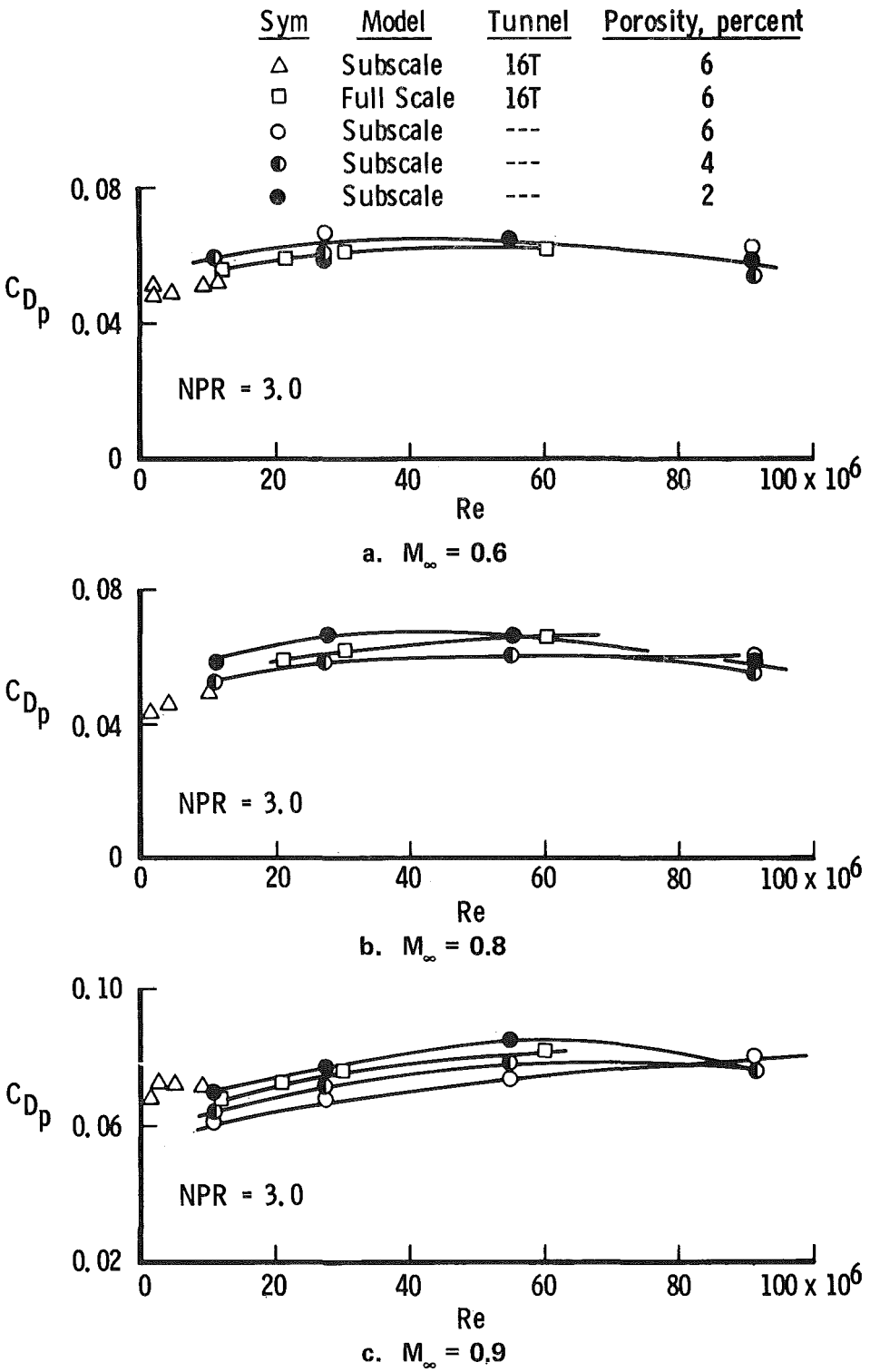

Figure 12. Drag coefficient as a function of Reynolds number for three test section wall porosities, Phase II.

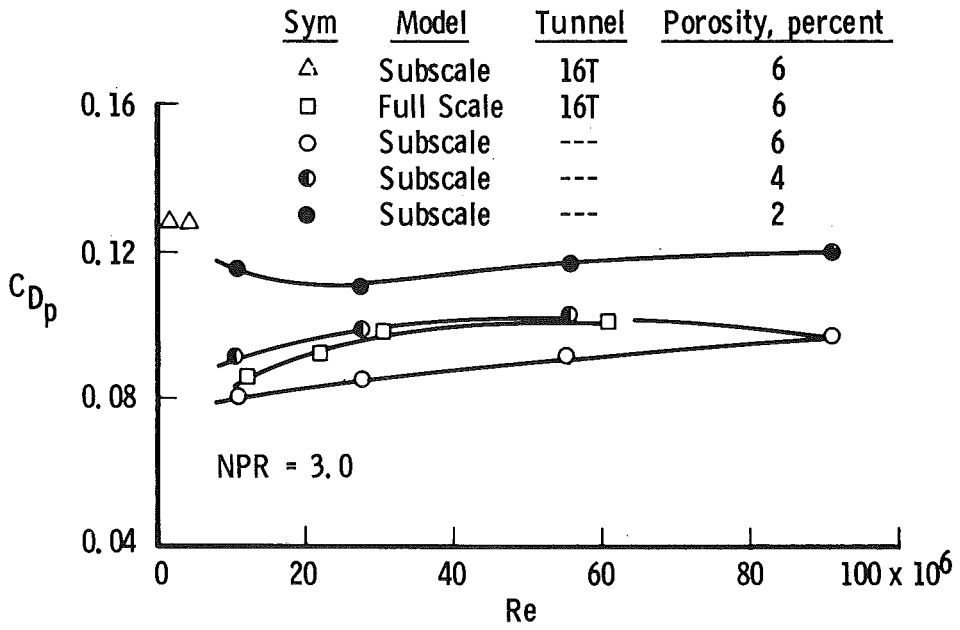

d. M_∞ = 0.95

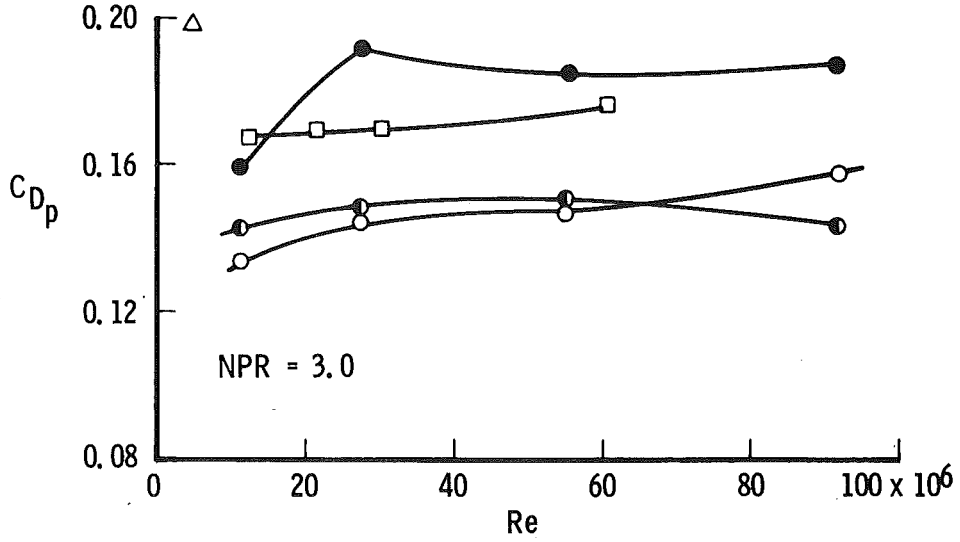

e. M_∞ = 1.1

Figure 12. Concluded.

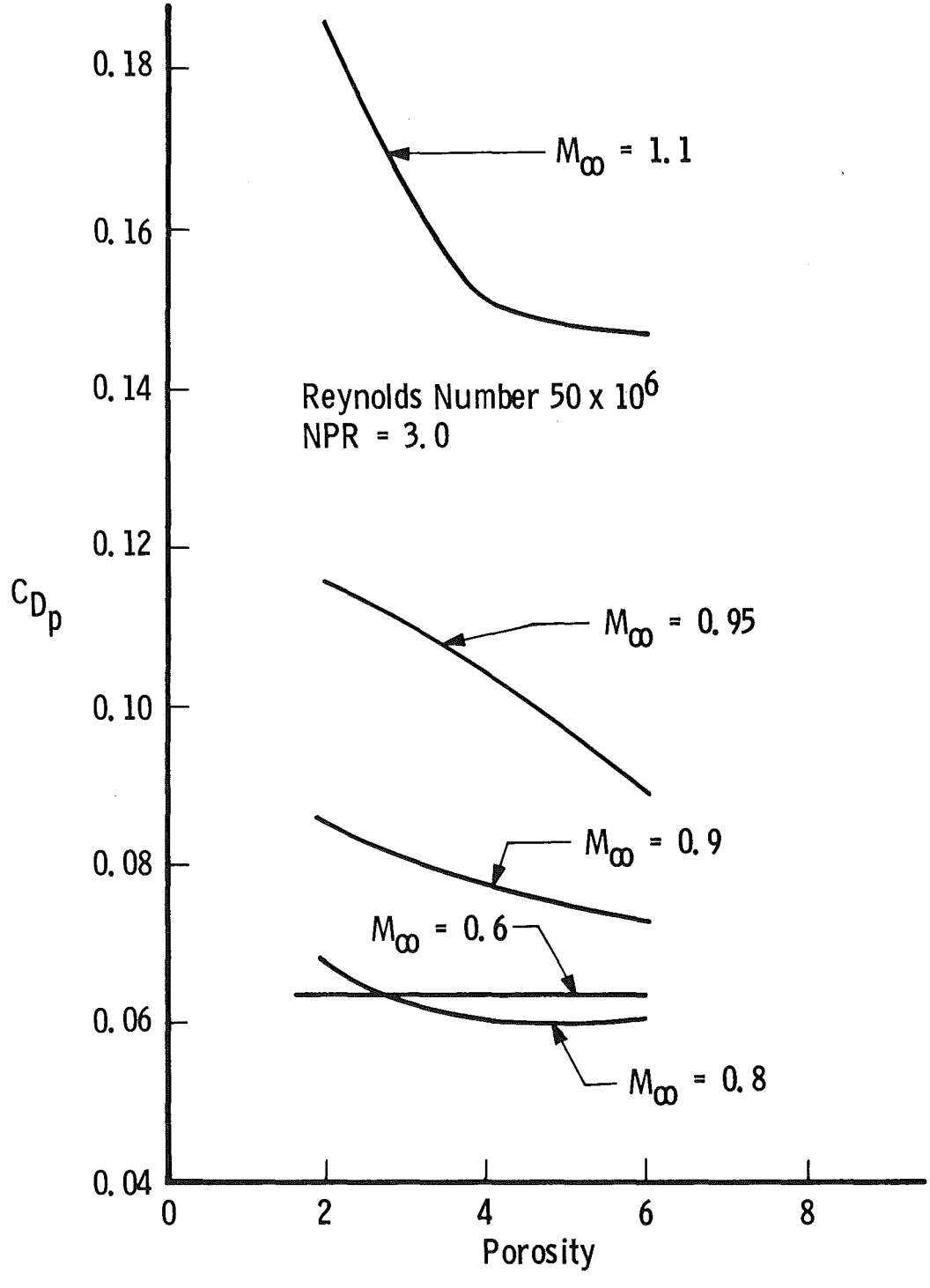

Figure 13. Effect of wall porosity on afterbody drag at Mach numbers from 0.6 through 1.1, Phase II.

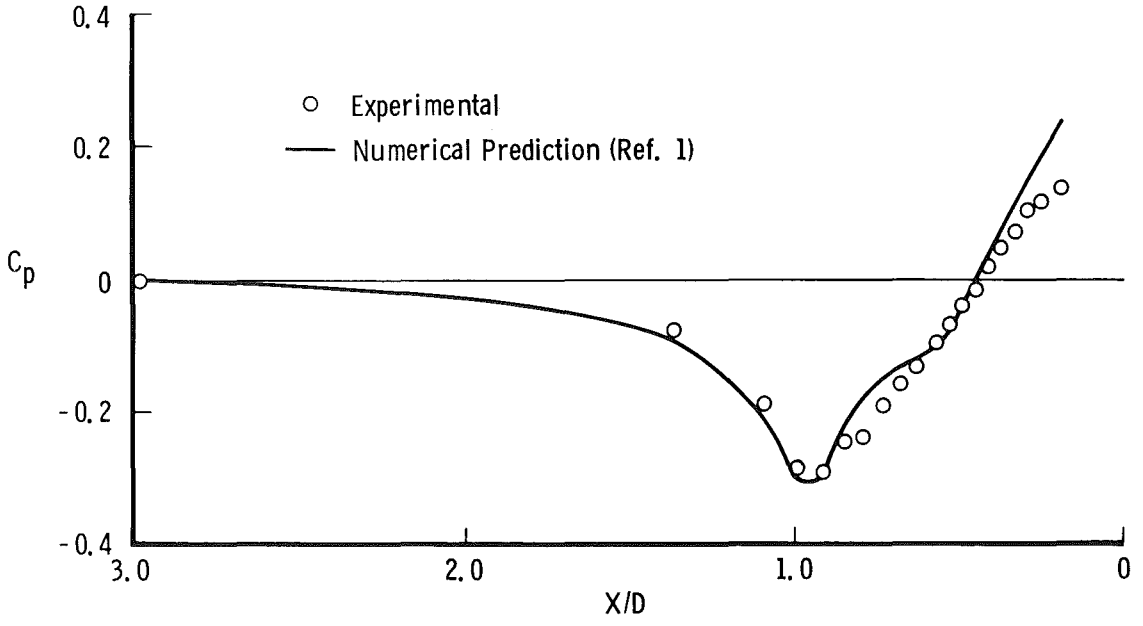

a. Re = 11 x 10^6

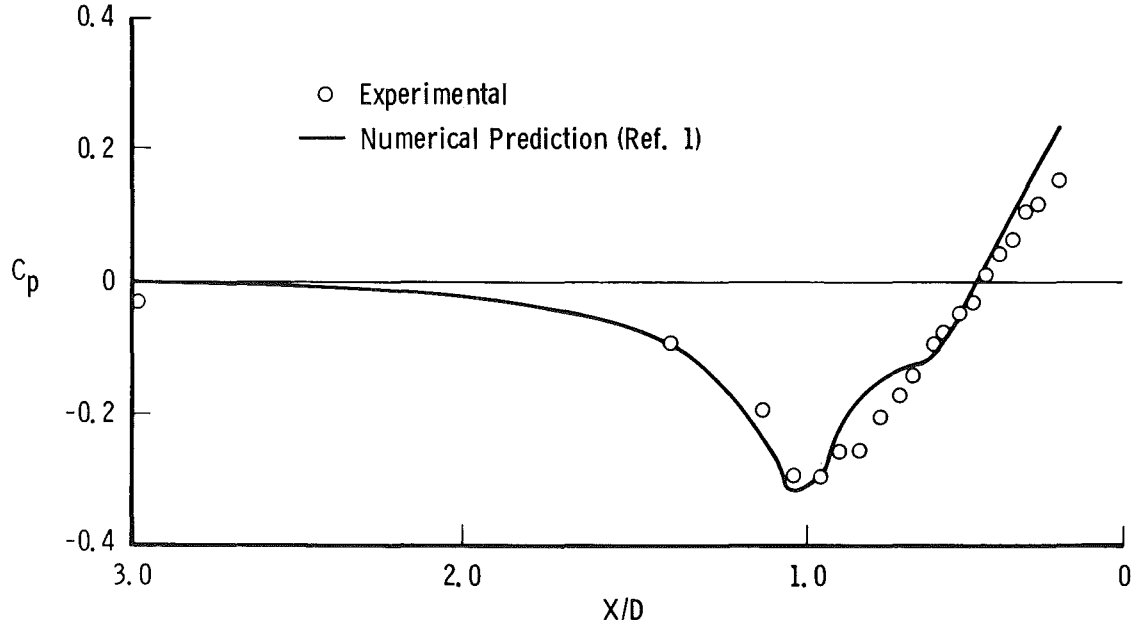

b. Re = 92 x 10^6

Figure 14. Comparison of numerical prediction with experimental pressure distribution at Mach 0.6.

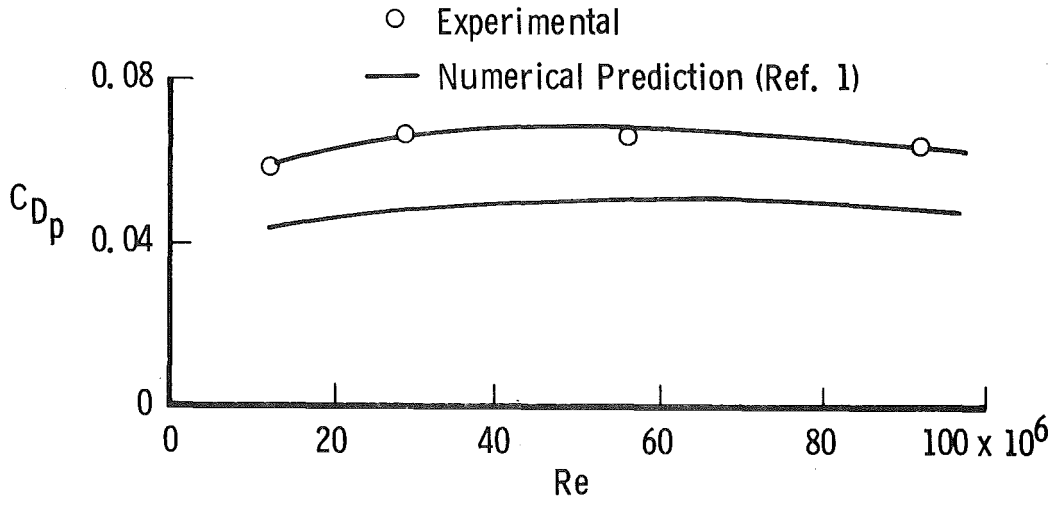

Figure 15. Comparison of drag coefficient determined from experimental pressure distribution and numerically determined pressure distribution at Mach 0.6.

5.0 SUMMARY OF RESULTS

An experimental investigation was conducted to study the effects of Reynolds number variation on isolated nozzle afterbody performance. Results of the investigation are summarized as follows:

1. The effect of Reynolds number variation on drag coefficient for the isolated AGARD Phase I and Phase II models was to increase C_{D_p} with increasing Reynolds number. The largest effect occurred at the highest Mach number.

2. The afterbody closure angle influences the effect of Reynolds number on C_{D_p}. The smallest change in C_{D_p} with varying Reynolds number was determined for the 10-deg afterbody. The 25-deg afterbody produced separated flow at all Mach number conditions and produced different characteristics with Reynolds number variation as the Mach number was varied.

3. In the Lockheed-Georgia CFF, the absolute value of drag coefficient was affected by tunnel wall porosity at Mach number 0.80 and above. The effect increased with increasing Mach number and produced the largest variations at Mach number 1.1.

4. Existing numerical techniques were used to predict NAB performance at Mach 0.6 and Reynolds numbers from 11 to 92 x 10^6. The pressure distribution determined numerically agreed well in the expansion region of the flow; however, the numerically predicted recompression was steeper than that measured experimentally.

5. Nozzle afterbody drag coefficient obtained by integration of the numerical predictions exhibited the same trend with increasing Reynolds number as did the experimental results; however, the absolute level of the coefficients was not the same.

REFERENCES

1. Galigher, L. L., Yaros, S. F., and Bauer, R. C. "Evaluation of Boattail Geometry and Exhaust Plume Temperature Effects on Nozzle Afterbody Drag at Transonic Mach Numbers." AEDC-TR-76-102.

2. Peters, W. L. "An Evaluation of Jet Simulation Parameters for Aircraft Engines at Transonic Mach Numbers." AEDC-TR-76-109.

3. Jackson, F. M. "Tunnel 16T Calibration for Nozzle Afterbody Research." Presented at the Forty-Fourth Semi-Annual Meeting of the Supersonic Tunnel Association, September 1975.

4. Pounds, G. A. and Stanewsky, E. "The Compressible Flow Facility, Part 1, Design." Lockheed-Georgia Company ER-9219-1, October 1971.

5. Robinson, C. E. and High, M. D. "Exhaust Plume Temperature Effects on Nozzle Afterbody Performance over the Transonic Mach Number Range." AEDC-TR-74-9 (AD781377), July 1974.

6. Laughrey, J. A. "Comparison of Testing Techniques for Isolated Axisymmetric Exhaust Nozzles in Transonic Flow." AIAA Paper 75-1292, AIAA/SAE 11th Propulsion Conference, Anaheim, California, September 29 - October 1, 1975.

7. Reubush, D. "The Effect of Reynolds Number on Boattail Drag." AIAA Paper No. 75-63, AIAA 13th Aerospace Sciences Meeting, Pasadena, California, January 20 - 22, 1975.

NOMENCLATURE

AREF	Reference area (based on maximum body diameter), ft^2
C_{D_p}	Drag coefficient (pressure integration, based on AREF), lbf
C_p	Static pressure coefficient, $(p_i - p_\infty)/q_\infty$
D	Maximum body diameter, in.
L	Model axial length, in.
MS	Model station, measured from nose, in.
M_∞	Free-stream Mach number
NPR	Nozzle pressure ratio, P_{T_j}/p_∞
NS	Nozzle station, in.
p_i	Local surface pressure, psia
P_{T_j}	Nozzle exhaust total pressure, psia
p_∞	Free-stream static pressure, psia
q_∞	Free-stream dynamic pressure, psia
Re	Reynolds number, based on model length
R_i	Local model radius, in.
L/D	Model axial length to diameter ratio
X/D	Ratio of distance from nozzle exit plane to model maximum diameter